Inhibition of human nasopharyngeal carcinoma growth and metastasis in mice by adenovirus-associated virus–mediated expression of human endostatin

Xiang-Ping Li,[1] Christine Y.S. Li,[4] Xiaohua Li,[1] Yanqing Ding,[1] Lally L.Y. Chan,[4] Pai-Hao Yang,[4] Gang Li,[1] Xiong Liu,[1] Jennifer S. Lin,[4] Jide Wang,[2] Mingliang He,[5] Hsiang-fu Kung,[5] Marie C. Lin,[4] and Ying Peng[3]

Departments of [1]Otolaryngology and [2]Gastroenterology, Nanfang Hospital, Nanfang Medical University; [3]Department of Neurology, The Second Affiliated Hospital, Sun Yat-Sen University, Guangzhou, China; [4]Department of Chemistry, Open Laboratory of Chemical Biology of the Institute of Molecular Technology for Drug Discovery, The University of Hong Kong; and [5]Li Ka Shing Institute of Health Sciences and Centre for Emerging Infectious Diseases, The Chinese University of Hong Kong, Hong Kong, China

Abstract

Nasopharyngeal carcinoma (NPC) is a highly malignant and frequently metastasized tumor. Endostatin has been shown to inhibit NPC growth, but its efficacy against NPC metastasis has not been shown *in vivo*. Here, we established a NPC metastasis model in mice by transplanting EBV-positive NPC cells, C666-1, in the livers of nude mice and observed lung metastasis. Furthermore, we showed that tail vein injection of recombinant adeno-associated virus encoding human endostatin (rAAV-hEndo) significantly prolonged the median survival rate of NPC metastasis–bearing mice (from 22 to 37 days, $P < 0.01$). The rAAV-hEndo treatment resulted in a statistically significant reduction in tumor growth and microvessel formation. It also increased the apoptotic index in the primary liver tumor but not in the normal liver tissue. Importantly, no formation of liver or lung metastasis was detected. The potent inhibition of NPC metastasis suggests the feasibility of combining rAAV-hEndo gene therapy with other therapies for the prevention and treatment of NPC metastasis. [Mol Cancer Ther 2006;5(5):1290–8]

Received 8/30/05; revised 1/25/06; accepted 3/2/06.

Grant support: The Guangdong Natural Science Fund, China (04020406, to X-P. Li and Y. Peng); the National Natural Science Fund of China (30471945 to X-P. Li); the Science and Technology Program of Guangdong province (2003c30303 to X-P. Li and Y. Peng); Li Ka Shing Institute of Health Sciences, and the Innovation and Technology Fund (ITS/084/03, H-F. Kung); this work is partially supported by the Foundation of Guangzhou Science and Technology Bureau (2005Z1-E0131 to H-F. Kung).

The costs of publication of this article were defrayed in part by the payment of page charges. This article must therefore be hereby marked advertisement in accordance with 18 U.S.C. Section 1734 solely to indicate this fact.

Requests for reprints: Marie C. Lin, Department of Chemistry, 8/F Kadoorie Biological Science Building, The University of Hong Kong, Pokfulam, Hong Kong, China. Phone: 852-2299-0776; Fax: 852-2817-1006. E-mail: mcllin@hkusua.hku.hk

doi:10.1158/1535-7163.MCT-05-0348

Introduction

Nasopharyngeal carcinoma (NPC) is a tumor derived from epithelial cells located in the posterior part of the nasopharynx. It is a highly malignant tumor which can easily invade local tissues and metastasize to distant organs such as the liver, lung, and brain. In the year 2000, >80% of new cases registered worldwide were reported from Southeast Asia (1), with the highest incident rate found in Southern China (~25–30 cases per 100,000 persons per year). Radiotherapy is the most common treatment for patients with NPC because it is highly sensitive to radiotherapy. Although the local control rate for NPC is approaching 90% (2), 30% to 40% of the patients with advanced stage NPC subsequently develop distant metastases and/or local recurrences (3). Most of the mortalities from patients with NPC are associated with secondary metastases of NPC in distant organs. The prognosis for patients with metastatic disease is poor, with a median survival of <12 months (4). No effective treatment for the metastasis of NPC is available; therefore, novel strategies are urgently needed.

Due to the lack of suitable animal models, we have established a nude mice model of NPC metastasis. In this new model, we inoculated C666-1 in the liver as a single nodule which would subsequently metastasize to other parts of the liver as well as the lung. C666-1 are human EBV-positive NPC cells (5) which have high metastatic potential (6).

Antiangiogenesis molecules have been shown to be effective in reducing tumor growth and metastasis, and human endostatin is one of the most well-characterized antiangiogenesis agents. Endostatin, a 20 kDa fragment of collagen XVIII, has been shown to induce apoptosis and inhibit the proliferation and migration of endothelial cells (7–10). Long-term treatment with endostatin has been shown to be essential (7, 11, 12), and a continuous administration of recombinant endostatin protein from an i.p. implanted osmotic pump could further reduce the dosage requirement and increase efficacy (13). These results suggest that sustained systemic concentration of the endostatin protein has advantages over daily bolus administration. Currently, clinical trials with recombinant human endostatin protein have already begun (12, 14–17); however, the requirement for a frequent dosing regimen and high dosages of expensive recombinant protein hinders future clinical applications (14).

In this study, we investigated the efficacy of recombinant type 2 adeno-associated virus encoding human endostatin (rAAV-hEndo) in the treatment of NPC metastasis in our mice models. We showed for the first time that long-term expression of endostatin by rAAV-hEndo is an effective method for preventing and treating NPC metastasis. The potential beneficial effects of supplementing rAAV-Endo gene therapy with radiotherapy and other therapies, for the treatment and prevention of NPC metastasis, warrant further investigations.

Materials and Methods

Cell Lines and Culture Conditions

The EBV-positive NPC cells, C666-1, were kindly provided by Dr. Dolly P. Huang from the Chinese University of Hong Kong (Hong Kong, China). ECV304, derived from human umbilical vein endothelial cells were obtained from American Type Culture Collection (Manassas, VA). Both cell lines were cultured in RPMI 1640 with 1% fetal bovine serum. HEK-293FT cells (Invitrogen, San Diego, CA) were cultured in DMEM (Life Technologies, Grand Island, NY) with 10% fetal bovine serum.

Preparation of the rAAV-hEndo and rAAV-Enhanced Green Fluorescence Protein Vectors

Plasmid pAAV-hEndo was constructed by inserting the human endostatin gene into the multiple cloning site of the AAV2 vector (ITR - cytomegalovirus promoter - β-globin intron - MCS - hEndo - hGH.polyA - ITR). Plasmid pAAV-enhanced green fluorescence protein (EGFP) was similarly constructed by inserting the *EGFP* gene between the *Xho*I and *Eco*RI sites of AAV2. rAAV particles were produced using a helper virus–free system as previously described (18–20), with minor modifications. Briefly, rAAV vectors and helper plasmid pDG were cotransfected into HEK 293FT cells (American Type Culture Collection) by calcium phosphate precipitation method. Transfected cells were harvested 60 hours later. They were trypsinized and resuspended in Tris buffer (pH 8.0). After two cycles of freeze/thawing, they were centrifuged for 20 minutes at 12,000 rpm. The supernatant fraction containing the rAAV-hEndo or rAAV-EGFP particles was decanted. rAAV particles were purified by HiTrap Heparin column chromatography (Sigma, St. Louis, MO). Peak virus fractions were collected and dialyzed against PBS containing 1 mmol/L $MgSO_4$. Samples were then concentrated using a 100K-MicroSep Centrifugal Concentrator (Life Technologies, Carlsbad, CA). Viral titer was quantified by real-time PCR using the TaqMan Universal PCR kit (Applied Biosystems, Foster City, CA), with the forward primer, 5′-CGG CTG TTG GGC ACT GA-3′, and the reverse primer, 5′-CCG AAG GGA CGA AGC AGA AG-3′. Aliquot of viral stocks (2×10^{12} viral genomes/mL) were stored at −80°C until ready for use.

rAAV-Mediated Transgene Expression *In vitro* in Cell Lines

C666-1 cells (4×10^5) were plated onto 35 mm^2 culture dishes. After 24 hours, cells were infected with 5×10^4 rAAV-EGFP or rAAV-hEndo viral genomes/cell in RPMI 1640 for 10 hours, followed by incubation in RPMI medium containing 10% fetal bovine serum. Forty-eight hours after infection, the expression of EGFP and hEndo was confirmed by fluorescence microscopy and Western blotting. The infection efficiency of rAAV-EGFP was calculated from the formula: infectious efficiency = (number of cells expressing green fluorescence / number of total cells) × 100%. The culture media of the transduced cells were collected for the analysis of human endostatin secretion. The *in vitro* studies were done at least thrice with reproducible results. Data from a representative experiment are shown.

Analysis of Protein Expressions by Western Blotting and Immunofluorescence

For Western blotting analysis of human endostatin, proteins were resolved by electrophoresis on 15% SDS-polyacrylamide gels, electroblotted onto Hybond-P membranes (Amersham Biosciences, Buckinghamshire, United Kingdom), and endostatin was detected by rabbit anti-endostatin (Abcam, Cambridge, United Kingdom). For immunofluorescence analysis of endostatin protein, cells were transduced with rAAV-hEndo for 48 hours, fixed with 3.7% formaldehyde, and permeabilized with 0.1% Triton X-100, then incubated with rabbit anti-human endostatin (1:50 dilution; NeoMarkers, Fremont, CA) at 37°C for 1 hour, and followed by incubating with FITC-conjugated goat anti-rabbit IgG (1:100 dilution; Zymed Laboratories, San Francisco, CA) at 37°C 1 hour. The fluorescence signals were observed by an inverted fluorescent microscope (Nikon TE300) with B-1A fluorescence filter set using an excitation filter of 450 to 490 nm, a dichromatic mirror of 505 nm, and a barrier filter of 520 nm. Pictures were taken using a Nikon F70.

Cell Proliferation and Apoptosis

Cell proliferation was measured by 3-(4,5-dimethylthiazol-1-yl)-2,5-diphenyltetrazolium bromide assay. ECV304 cells (5×10^3/well) were plated onto 96-well plates and maintained in 80 μL of RPMI 1640 (supplemented with 1% fetal bovine serum and 3 ng/mL of vascular endothelial growth factor; Peprotech, Rocky Hill, NJ) to 70% confluency. Then, cells were treated with 20 μL of conditioned medium which was collected from C666-1 cells either infected with rAAV-hEndo (hEndo group), rAAV-EGFP (control group 2), or noninfected cells (control group 1). Six replicates were done for each group. After 24, 48, and 72 hours of incubation, 20 μL of 3-(4,5-dimethylthiazol-1-yl)-2,5-diphenyltetrazolium bromide (5 mg/mL) was added to each well, and the incubation was maintained for an additional 4 hours at 37°C. At the end of the incubation period, 150 μL of DMSO was added to each well and thoroughly mixed for 10 minutes. The UV absorbance at 570 nm was then determined.

Flow Cytometry and Terminal Deoxynucleotidyl Transferase–Mediated dUTP Nick-End Labeling Staining

ECV304 cells were first infected with rAAV-hEndo or rAAV-EGFP. Cells were then collected after 48 hours and

fixed in ice-cold (−70°C) ethanol for 24 hours. After resuspension in PBS, they were digested with RNase (100 μL/mL) at 37°C for 30 minutes, and then incubated with propidium iodide (50 μg/mL) for 20 minutes. Five thousand cells from each sample were analyzed by flow cytometry (Coulter Epics, XL, High Wycombe, United Kingdom). For terminal deoxynucleotidyl transferase–mediated dUTP nick-end labeling (TUNEL) assay, ECV304 cells transduced with rAAV-hEndo or rAAV-EGFP were fixed and permeabilized. The TUNEL assay was done according to the manufacturer's instructions. Cells that stained brown were scored as apoptotic cells. The number of apoptotic cells were quantified on five randomly selected visual fields under a light microscope on 400× magnification. The apoptotic index was calculated by the formula: apoptotic index = (total number of apoptotic cells / total number of nucleated cells) × 100%.

Animal Model of NPC Metastasis and Experimental Conditions

Male nude mice (BALB/c *nu/nu*, 5–7 weeks old, 15–22 g in weight) were purchased from Charles River Labs (Wilmington, WA). Mice were maintained under pathogen-free conditions (specific pathogen-free level). Then mice were anaesthetized with 1% pentobarbital sodium (40 mg/kg) before surgery. Primary tumors were established by direct injection of 2×10^7 C666-1 either s.c. or directly into the liver as indicated. The rAAV and PBS treatments were administrated either intratumorally or i.v. through tail vein. The survival rate was recorded everyday and survival curves were constructed and analyzed by a log-rank test. The *in vivo* studies were done at least thrice with reproducible results. Data from a representative experiment are shown.

To determine the minimal effective therapeutic dosage of rAAV-hEndo *in vivo*, we randomly divided the NPC-bearing nude mice into four groups ($n = 4$ per group) and injected, through the tail vein, a total of 2.5×10^{10}, 0.5×10^{11}, and 1.5×10^{11} viral genomes of AAV-hEndo in two equal doses at days 1 and 8 after tumor inoculations. Mice survival rates were monitored. The median survival rates were 25 ± 4, 29 ± 3, and 36 ± 4, respectively. Therefore, we chose the 1.5×10^{11} viral genomes AAV-hEndo in two injections as the treatment dosage for subsequent studies.

Pathology and Immunohistochemical Analysis

The tumor volume, accumulation of ascites, and degree of tumor metastasis were evaluated. Livers and lungs of the treated mice were excised and fixed in 4% paraformaldehyde and paraffin-embedded. Tissue sections were stained with H&E. The longest (a) and shortest diameters (b) of the xenografted tumor were measured. Tumor volume, $V = ab^2 \times 0.52$. The rate of growth inhibition of xenografted tumor was calculated by the formula: growth inhibition = $[(V_{\text{control group}} - V_{\text{experimental group}}) / V_{\text{control group}}] \times 100\%$.

Tissue sections from paraffin blocks were cut, dewaxed, and hydrated. Antigens were retrieved by heating in the microwave. Sections were then treated with 3% hydrogen peroxide for 10 minutes, and incubated with antiendostatin primary antibody for 1 hour. After washing with PBS, they were further incubated with the horseradish peroxidase–conjugated secondary antibody for 30 minutes and stained with 3,3′-diaminobenzidine solution. Intratumoral microvessels were stained with a monoclonal antibody against the CD34 antigen on endothelial cells for the assessment of intratumoral microvessel density. Results were evaluated using the Weidner standard (21) of scoring. Neovascular ''hotspots'' with the highest microvessel density were identified using light microscopy (40× fields). Three fields under 200× magnification in the hotspot were randomly chosen for each specimen. The number of microvessels was counted and microvessel density was calculated.

Statistical Analysis

One-way ANOVA was used for statistical analyses. Log-rank tests were done for survival curves. Results were expressed as mean ± SD. $P < 0.05$ was considered statistically significant. Data were analyzed with SPSS 10.0 software (SPSS Advanced Models 10.0, SPSS, Inc., Chicago, IL).

Results

Expression of Human Endostatin by rAAV-hEndo Infection *In vitro*

To determine the infectious efficiency of the rAAV serotype 2 in human endothelial cells, ECV304 and human EBV-positive NPC cells, C666-1, were infected with rAAV-EGFP at 5×10^2, 5×10^3, or 5×10^4 viral genomes/cell in a dose-dependent manner to produce a fluorescence signal after 24 hours of infection, with maximum fluorescence observed after 48 hours. The highest infectious efficiency (95%) was obtained 48 hours postinfection with a multiplicity of infection of 5×10^4 (Fig. 1A). The transduction of rAAV-hEndo to C666-1 cells was evaluated by immunofluorescence (Fig. 1B and C), which showed strong fluorescent signals in the cytoplasm. To further test infectious efficiency, the conditioned medium of rAAV-hEndo infected cells was subjected to Western blot analysis, revealing the presence of human endostatin in the conditioned medium of rAAV-hEndo infected cells (*lanes 1–4*, Fig. 1D), but not in cells infected with rAAV-EGFP (*lanes 5–8*, Fig. 1D) or PBS (data not shown). These results showed the high transduction efficiency of rAAV-hEndo in ECV304 and C666-1 cells, as well as the expression/secretion of human endostatin protein.

Because endostatin could inhibit the growth of the tumor vasculature, rAAV-hEndo infection was then tested for direct programmed cell death induction in ECV304 cells. ECV304 cells were transduced with rAAV-hEndo or rAAV-EGFP for 48 hours. TUNEL staining revealed that rAAV-EGFP-infected cells (4.2 ± 1.9%) and PBS-treated cells (4.0 ± 0.8%) both exhibited low apoptotic indices (Fig. 1E and H). In contrast, rAAV-hEndo-infected cells (Fig. 1F) exhibited a significantly higher (8-fold) apoptotic index (32.6 ± 3.2%, $P < 0.01$) when compared with the control cells. The nucleus of the apoptotic cells appeared condensed and fragmented (Fig. 1G).

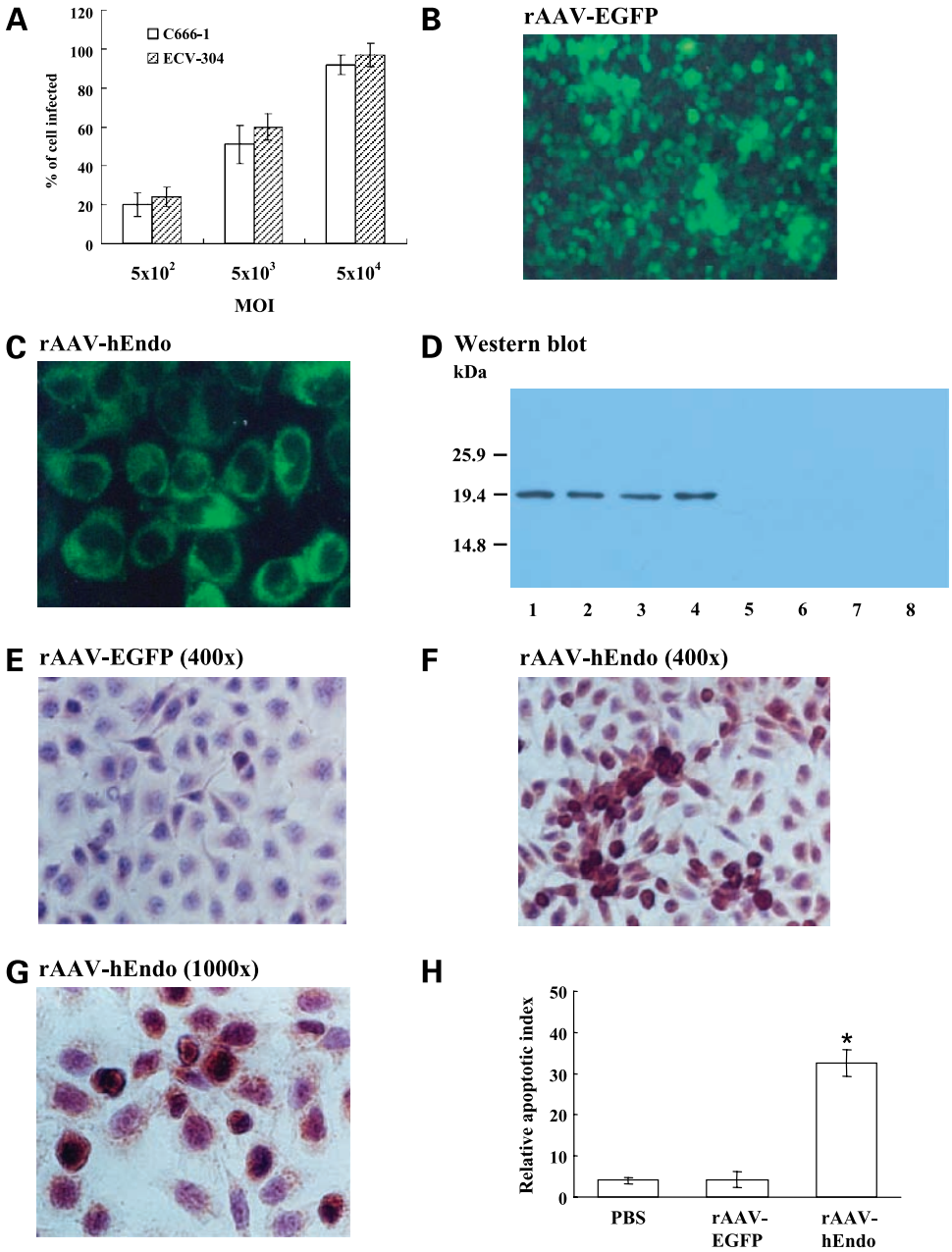

Figure 1. Infection of C666-1 and ECV-304 cells by rAAV viruses. **A,** different viral dosages were used to infect the cells (*C666-1* and *ECV-304*) to determine transduction efficiency. **B,** C666-1 cells were infected with rAAV-EGFP (5×10^4 viral genomes/cell) for 48 h (original magnification, ×100). **C,** ECV-304 cells were infected with 5×10^4 viral genomes/cell of rAAV-hEndo for 48 h (original magnification, ×1,000). **D,** identification of human endostatin in the C666-1 (*lanes 1, 3, 5,* and *7*) and ECV-304 (*lanes 2, 4, 6,* and *8*) cultures by Western blot. Cell lysate from cells infected with rAAV-Endo (*lanes 1* and *2*) and from cells infected with rAAV-EGFP (*lanes 5* and *6*). Condition medium from cells infected with rAAV-Endo (*lanes 3* and *4*) and from cells without treatment (*lanes 7* and *8*). **E,** TUNEL staining of untreated ECV-304 at low magnification (×400); cells infected with rAAV-hEndo at low (×400; **F**) and high magnification (×1,000; **G**). **H,** relative apoptotic indices were compared between the rAAV-hEndo and rAAV-EGFP infection. *, $P < 0.01$ compared with PBS.

Inhibition of VEGF-Induced ECV-304 Proliferation by the Culture Medium from rAAV-hEndo-Infected C666-1

Previous Western blot analyses have shown that the conditioned medium contained endostatin protein secreted by the rAAV-hEndo-infected cells. 3-(4,5-Dimethylthiazol-1-yl)-2,5-diphenyltetrazolium bromide assay was then done to examine whether this conditioned medium could inhibit VEGF-induced proliferation of ECV-304. The number of viable cells was significantly decreased (67.3%, $P < 0.01$) in the medium from rAAV-hEndo-infected C666-1 (Fig. 2A). To understand the mechanism involved in growth reduction, flow cytometry analysis was done on the cell cycle profile of the rAAV-hEndo-transfected ECV304, which showed a significantly higher percentage of cells in the G_1 phase (74.3 ± 8.5%, $P < 0.01$; Fig. 2B and D) than the control rAAV-EGFP-infected medium (49.6 ± 8.0%; Fig. 2C and D).

Establishment of NPC Metastasis Model in Mice

To evaluate the antimetastatic effect of rAAV-hEndo, a NPC metastasis model in nude mice was established. In order to establish a NPC metastasis animal model, we initially attempted to inoculate C666-1 cells directly into the mice or rat nasopharyngeal tissue. However, it was difficult to establish the technique. Our second attempt was to inject cells into the carotid triangle area, but we

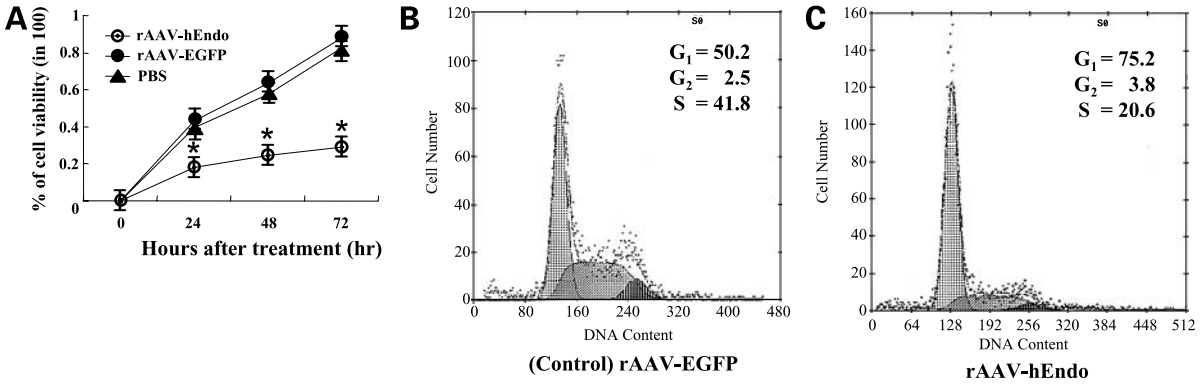

D

Cell cycle	% G_1	% G_2	% S
Control (n=3)	49.6 ± 8.0	8.2 ± 6.4	42.2 ± 7.8
rAAV-hEndo (n=3)	74.3 ± 8.5[a]	4.0 ± 2.4	21.7 ± 4.0[a]

[a] $P < 0.01$, significantly different from the control values

Figure 2. Effect of human endostatin on cell proliferation. **A,** growth curves for ECV304 cells incubated with conditioned medium obtained from C666-1 infected with rAAV-hEndo (○), rAAV-EGFP (●), and PBS (▲). Cell proliferation was measured by 3-(4,5-dimethylthiazol-1-yl)-2,5-diphenyltetrazolium bromide assay. Values represent the mean ± SD of three independent experiments; *, $P < 0.01$ compared with mock infection and rAAV-EGFP-treated groups. Flow cytometry analyses of ECV-304 cells infected with (Control) rAAV-EGFP (**B**) and rAAV-hEndo (**C**). **D,** different cell cycles were compared between control and rAAV-hEndo.

failed to observe metastasis. Finally, we inoculated C666-1 cells into the liver and found that this strategy consistently produced a single NPC tumor nodule at the injection site. In addition, the tumor cells metastasized to other parts of the liver, and then to the lung.

Primary tumors were established by direct injection of 2×10^7 C666-1 cells into the liver of nude mice as a single nodule under direct visualization after laparotomy. Seven days after inoculation, primary tumors were successfully established (100%) in the livers of all of the nude mice examined. By day 21, all of the examined nude mice ($n = 3$) had shown a single large round primary liver tumor at the original injection site, with liver metastasis (100%) and marked lung metastasis (60%).

rAAV-hEndo Treatment Prolonged Survival Rate of Mice Bearing NPCs in the Liver

To determine whether rAAV-hEndo therapy could prolong the survival rate of mice, primary tumors were established by direct injection of 2×10^7 C666-1 into the liver as previously described. Twenty-four hours after inoculation, mice were divided into three treatment groups ($n = 12$/group). The rAAV-hEndo (0.1 mL, 1.5×10^{11} viral genomes), rAAV-EGFP (0.1 mL, 1.5×10^{11} viral genomes), and PBS (0.1 mL) were given i.v. through the tail vein. A second administration was carried out similarly 8 days after tumor inoculation. Six mice from each group were randomly chosen for long-term survival study on day 10. The remaining six mice were sacrificed on day 21, and tissues were collected for pathologic and immunohistochemical analysis. The survival curves of each group are shown in Fig. 3. In this nude mice study, the average survival period of the rAAV-hEndo treatment group was significantly longer (36.50 ± 8.46 days) than the rAAV-EGFP treatment (24.00 ± 5.66 days) and PBS treatment (21.17 ± 3.92 days) groups ($P < 0.01$). In this case, different doses of viral vectors were evaluated in the nude mice model (data not shown).

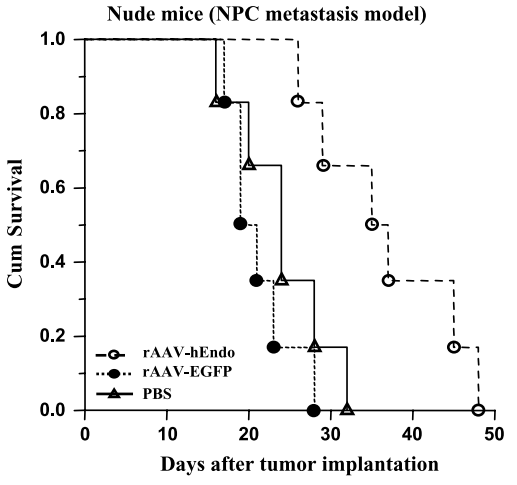

Figure 3. rAAV-hEndo treatment prolonged the survival of NPC-bearing mice. The experimental conditions stated in the text. The rAAV-hEndo (○), rAAV-EGFP (●), and PBS (▲) treatments were given i.v. through the tail vein. The survival rate was recorded everyday and the survival curve was constructed and analyzed by a log-rank test.

rAAV-hEndo Treatment Inhibited Primary Tumor Growth and Prevented Liver and Lung Metastasis

Liver morphologies from all three groups in nude mice NPC metastasis study were evaluated 21 days after tumor inoculation. In the nude mice study ($n = 6$), livers from the control rAAV-EGFP (Fig. 4B) and PBS (Fig. 4C) treatment groups displayed multiple metastasized tumors of different sizes on the surface of the liver (*open arrowhead*). In contrast, the surface of livers in rAAV-hEndo-treated mice (Fig. 4A) was smooth (*open arrowhead*) with no sign of liver metastasis, except for the region containing the transplanted tumor (*solid arrow*). All of the transplanted tumors appeared round-shaped, and grew on the surface of the liver (*solid arrows*, Fig. 4A–C). The lung morphology was also evaluated on day 21. As shown in Fig. 4D, rAAV-hEndo-treated mice showed normal lung morphology with no indication of tumors, whereas the control rAAV-EGFP treated (Fig. 4E) and PBS treated (Fig. 4F) mice clearly showed multiple lung tumors (*small arrows*). As shown in Table 1, when the rAAV-hEndo-treated group was compared with the control rAAV-EGFP- and PBS-treated groups, the volumes of the xenografted primary liver tumors were significantly reduced by 63% ($P < 0.05$) and 71% ($P < 0.01$), respectively. In contrast, no significant difference was found between the tumor volumes of the two control rAAV-EGFP- and PBS-treated groups ($P > 0.05$). No liver or lung metastasis was observed in the rAAV-hEndo-treated group, whereas the AAV-EGFP- and PBS-treated groups displayed liver metastasis of 100%, accompanied by lung metastases of 50% and 67%, respectively. In addition, AAV-hEndo treatment also significantly inhibited the development of ascites fluid accumulations.

The liver and lung morphologies of AAV-hEndo-treated mice at the time of death (days 30–40) were also examined. As shown in Fig. 4G, a large single nodule of primary tumor mass was found with no indication of liver metastasis in all the mice that were examined. Liver sections from the middle of the tumor mass revealed large necrotic tissues (Fig. 4H). Furthermore, no lung metastasis was found in all six mice that were examined (Fig. 4I).

rAAV-hEndo Treatment Decreased Intratumoral Vascularization and Induced Tumor Necrosis and Apoptosis

H&E staining showed that the rAAV-hEndo treatment produced large areas of necrosis in the primary tumor tissues (*black arrow*, Fig. 5A). In contrast, few necrotic tissues were observed in the primary tumor of the rAAV-EGFP-treated (Fig. 5B) and PBS-treated (Fig. 5C) groups. Consistent with morphologic observations, the histologic studies confirmed the presence of metastasized tumors in lung tissues from the rAAV-EGFP-treated (Fig. 5E) and PBS-treated (Fig. 5F) groups. No tumor tissue was found in the lung of the rAAV-hEndo-treated group (Fig. 5D).

Immunohistochemical detection of CD34 in the tumor tissues also showed a significantly low microvessel density (3.67 ± 1.63) in the rAAV-hEndo-treated group (Fig. 6A), as compared with the two controls of rAAV-EGFP-treated (Fig. 6B) and PBS-treated (Fig. 6C) groups (19.67 ± 2.16 and 22.50 ± 3.02, respectively; $P < 0.01$). TUNEL staining was used to examine cell apoptosis in which the apoptotic cells were stained brown by *in situ* labeling of fragmented DNA. The primary tumors from the rAAV-hEndo-treated group exhibited 5- to 6-fold higher apoptotic indices ($28.83 \pm 5.27\%$, $P < 0.01$) when compared with the two controls of rAAV-EGFP-treated ($6.17 \pm 2.79\%$; Fig. 6E) and PBS-treated ($4.50 \pm 2.17\%$; Fig. 6F) groups.

Immunohistochemical analysis for human endostatin protein expression from the rAAV-hEndo-treated group showed strong positive signals in the liver tissues surrounding the blood vessel (Fig. 6G), whereas no signal was detected in the liver sections prepared from the two

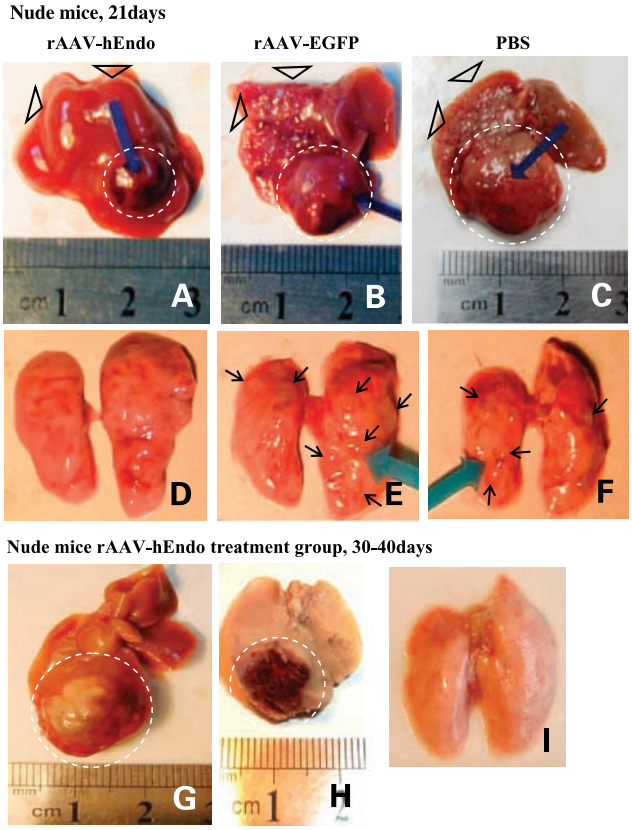

Figure 4. Gene therapy with rAAV-hEndo inhibited NPC primary tumor growth and prevented liver and lung metastasis. Photographs were taken from nude mice 21 d after tumor inoculation. Liver morphology was examined from the treatment groups of rAAV-hEndo (**A**), rAAV-EGFP (**B**), and PBS (**C**). *Solid arrow,* site of the primary NPC tumors. *Open arrows,* signs of metastasis. Lung morphology at day 21, rAAV-hEndo treatment group with no visible tumor (**D**), rAAV-EGFP treatment (**E**) and PBS treatment groups (**F**) both showed multiple tumors (*small arrows*). Photographs were taken from rAAV-hEndo-treated mice at the time of death (days 30–40). The morphologies of fresh intact liver (**G**), formalin-fixed liver (**H**), and fresh lung (**I**) were examined.

Table 1. Antitumor effects of rAAV-mediated endostatin therapy in NPC xenograft transplanted mice

Treatment group	No. of mice	Volume of transplanted tumor (cm^3, $\bar{x} \pm s$)	Development of ascites (%)	Metastases in liver (%)	Metastases to lung (%)
AAV-hEndo	6	0.481 ± 0.207*	16.7	0.0	0.0
AAV-EGFP	6	1.311 ± 0.437	100	100	50.0
PBS	6	1.644 ± 0.538	100	100	66.7

NOTE: Values represent mean ± SD. Significant differences were analyzed using one-way ANOVA with multiple comparisons.
*$P < 0.01$, significantly different from the rAAV-EGFP-treated and PBS-treated groups.

control groups (data not shown). This indicated that tail vein injection of rAAV-hEndo successfully delivered the human endostatin gene into the liver, and that human endostatin protein was expressed.

Discussion

It is well known that angiogenesis is directly involved in the growth and metastasis of a variety of solid tumors (22–27). Antiangiogenic therapy is expected to reduce intratumoral microvessel formation, which leads to a limited supply of blood reaching the tumor mass, as a result, suppressing tumor growth. Necrosis would similarly develop because of the inadequate supply of nutrients and oxygen, leading to hypoxia, ischemia, and apoptosis of the tumor cells in areas containing reduced numbers of microvessels. Inhibition of microvessel formation would also suppress metastases, which are dependent on angiogenesis (27).

Gene therapy, in which the synthesis of endostatin is directly localized within a patient's body, may provide an effective method with which to achieve long-term, continuous administration of the protein. Adenovirus-based vectors have been used extensively in gene delivery for antiangiogenic molecules. However, the transient effect, dose-dependent toxicity (28), and activation of CTL response (29) of adenovirus vectors are some of the major drawbacks. In addition to adenovirus, naked DNA, or plasmids carrying endostatin or other antiangiogenesis genes, have also been reported with limited efficacy (30–32). In our study, AAV was chosen as the delivery vehicle of human endostatin gene to treat NPC metastasis due to its nonpathogenicity, nonimmunogenic, and replication-defective characteristics (33, 34). In addition, its ability to mediate efficient and long-term gene transduction are observed not only in the liver but also across a broad range of dividing or nondividing mammalian tissues (35).

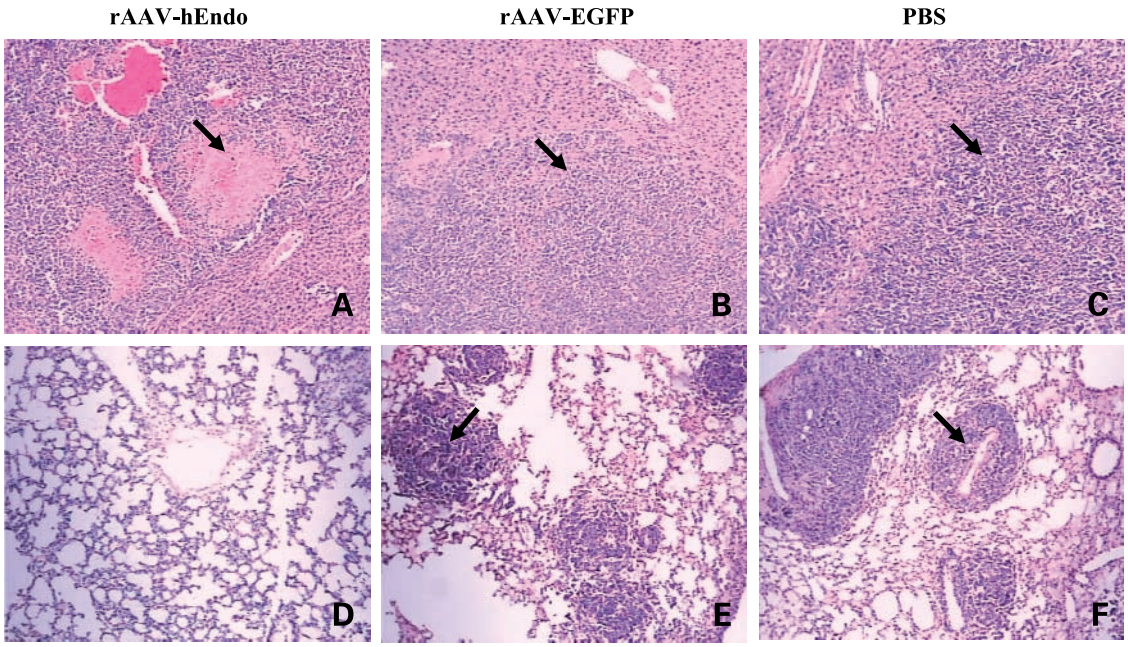

Figure 5. Detection of necrosis and metastasis after rAAV-hEndo treatment. Tissue sections of formalin-fixed, paraffin-embedded primary tumors were stained by H&E. **A,** liver primary tumor tissues from rAAV-hEndo-treated mice; *arrow,* one of the necrotic areas. rAAV-EGFP-treated mice (**B**) and PBS-treated mice (**C**); *arrows,* areas where tumor cells grew extensively. Lung tissues from rAAV-hEndo-treated mice (**D**), rAAV-EGFP-treated mice (**E**), and PBS-treated mice (**F**); *arrows,* tumors.

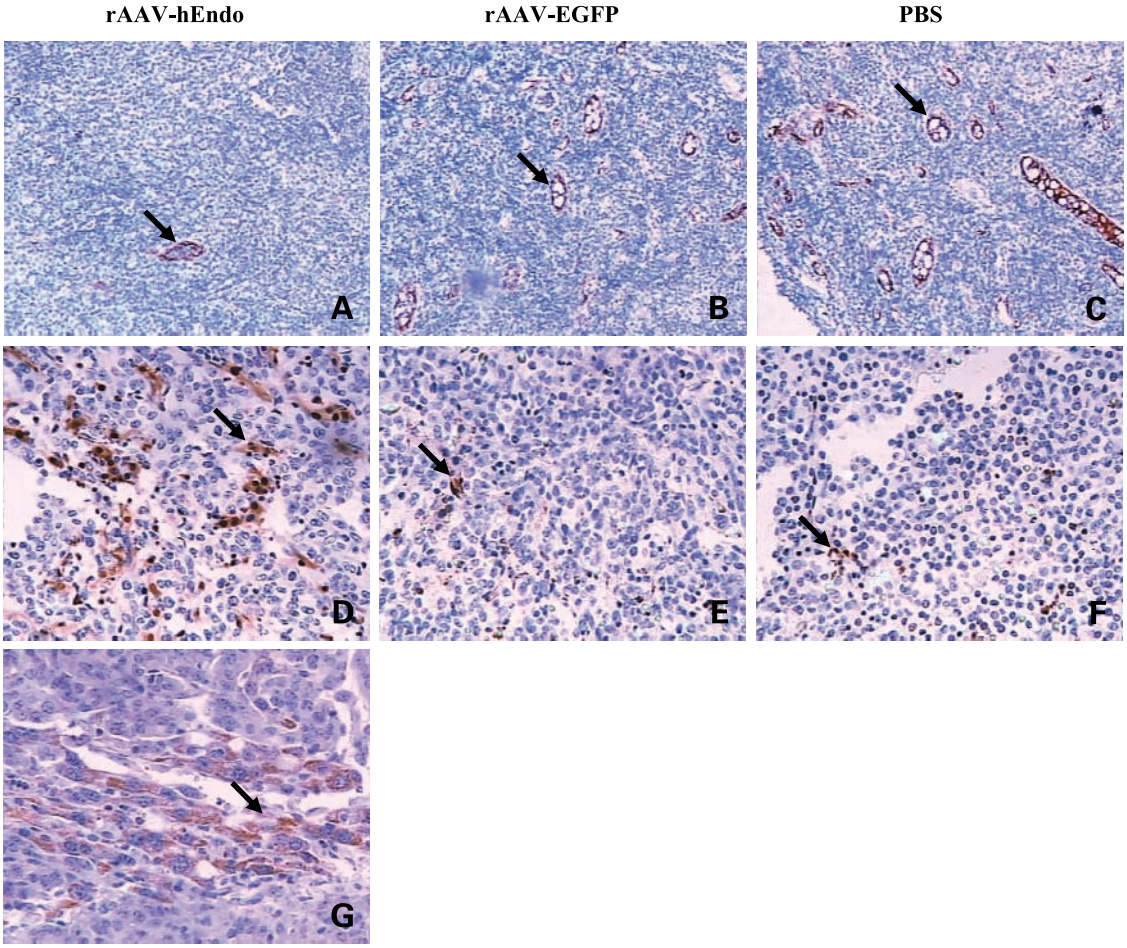

Figure 6. Detection of vascularization and apoptosis after rAAV-hEndo treatment. Tissue sections of formalin-fixed, paraffin-embedded primary liver tumors were immunohistochemically stained for CD34, or TUNEL-stained for the detection of apoptotic cells. Images are representative fields of view from tumors 21 d after treatment (original magnification, ×200). Immunohistochemical staining of CD34-positive microvessel of primary tumor tissues in rAAV-hEndo (**A**), rAAV-EGFP (**B**), and PBS treatment (**C**) groups. TUNEL staining from tumor tissue of hEndo-treated (**D**), EGFP-treated (**E**), and PBS-treated (**F**) groups (original magnification, ×200). **G,** immunohistochemical staining for the expression of human endostatin in liver tissues from rAAV-hEndo treatment group using the antihuman endostatin antibody.

We established a NPC metastasis model in nude mice. Using this model, we tested the therapeutic effect of rAAV-hEndo-mediated expression of human endostatin in NPC tumor growth and metastasis. Observations from our study showed that tail vein injection of rAAV-hEndo resulted in long-term expression of endostatin in the liver, accompanied with reduced NPC tumor growth and intratumoral microvessel density, increased tumor apoptosis and necrosis. More importantly, we have shown that rAAV-hEndo treatment significantly prolongs survival and prevents NPC metastasis.

In summary, this is the first *in vivo* preclinical study which shows that NPC metastasis is critically dependent on tumor angiogenesis, as rAAV-endostatin alone is sufficient to achieve the inhibition of NPC metastasis. This is consistent with previous clinical studies in patients with NPC (36), which shows that the increased intratumoral microvessel density was not only related to the metastatic potency of NPC (37), but also correlated with overall survival (38). With no effective treatments available for patients with NPC at the stage of metastasis, results from this study provide a basis for the future development of a cocktail therapy which will include radiotherapy, together with long-term endostatin therapy mediated by AAV and/or other gene delivery systems for the prevention and treatment of NPC metastasis.

Acknowledgments

We thank Prof. Dolly Huang for kindly providing the C666-1, and Dr. Rory Watt (University of Hong Kong) for critically reading this manuscript.

References

1. Ferlay J, Bray F, Pisani P, Parkin DM. GLOBOCAN 2000: cancer incidence, mortality and prevalence worldwide, version 1.0. IARC Cancer Base No. 5. Lyon: IARC; 2001.

2. Chua DT, Sham JS, Leung LH, Au GK. Re-irradiation of nasopharyngeal

carcinoma with intensity-modulated radiotherapy. Radiother Oncol 2005; 77:290 – 4.

3. Teo PM, Chan AT. Treatment strategy and clinical experience. Semin Cancer Biol 2002;12:497 – 4.

4. Ma BBY, Chan ATC. Recent perspectives in the role of chemotherapy in the management of advanced nasopharyngeal carcinoma. Cancer 2005; 103:22 – 31.

5. Cheung ST, Huang DP, Hui AB, et al. Nasopharyngeal carcinoma cell line (C666 – 1) consistently harbouring Epstein-Barr virus. Int J Cancer 1999;83:121 – 6.

6. Li XP, Li G, Peng Y, Kung HF, Lin MC. Suppression of Epstein-Barr virus-encoded latent membrane protein-1 by RNA interference inhibits the metastatic potential of nasopharyngeal carcinoma cell. Biochem Biophys Res Commun 2004;315:212 – 8.

7. Reilly MSO, Boehm T, Shing Y, et al. Endostatin: an endogenous inhibitor of angiogenesis and tumor growth. Cell 1997;88:277 – 85.

8. Yamaguchi N, Anand-Apte B, Lee M, et al. Endostatin inhibits VEGF-induced endothelial cell migration and tumor growth independently of zinc binding. EMBO J 1999;18:4414 – 23.

9. Skovseth DK, Veuger MJ, Sorensen DR, De Angelis PM, Haraldsen G. Endostatin dramatically inhibits endothelial cell migration, vascular morphogenesis and perivascular cell recruitment *in vivo*. Blood 2005; 105:1044 – 51.

10. Dhanabal M, Ramchandran R, Waterman MJ, et al. Endostatin induces endothelial cell apoptosis. J Biol Chem 1999;274:11721 – 6.

11. Boehm T, Folkman J, Browder T, O'Reilly MS. Antiangiogenic therapy of experimental cancer does not induce acquired drug resistance. Nature 1997;390:404 – 7.

12. Herbst RS, Hess KR, Tran HT, et al. Phase I study of recombinant human endostatin in patients with advanced solid tumors. J Clin Oncol 2002;20:3792 – 803.

13. Kisker O, Becker CM, Prox D. Continuous administration of endostatin by intraperitoneally implanted osmotic pump improves the efficacy and potency of therapy in a mouse xenograft tumor model. Cancer Res 2001; 61:7669 – 74.

14. Thomas JP, Arzoomanian RZ, Alberti D, et al. Phase I pharmacokinetic and pharmacodynamic study of recombinant human endostatin in patients with advanced solid tumors. J Clin Oncol 2003;21:223 – 31.

15. Eder JP, Jr., Supko JG, Clark JW, et al. Phase I clinical trial of recombinant human endostatin administered as a short intravenous infusion repeated daily. J Clin Oncol 2002;20:3772 – 84.

16. Mundhenke C, Thomas JP, Wilding G, et al. Tissue examination to monitor antiangiogenic therapy: a phase I clinical trial with endostatin. Clin Cancer Res 2001;7:3366 – 74.

17. Twombly R. First clinical trials of endostatin yield lukewarm results. J Natl Cancer Inst 2002;94:1520 – 1.

18. Chen Y, Luk KD, Cheung KM, et al. Gene therapy for bone formation using adeno-associated viral bone morphogenetic protein-2 vectors. Gene Ther 2003;10:1345 – 53.

19. Grimm D, Kern A, Rittner K, Kleinschmidt JA. Novel tools for production and purification of recombinant adenoassociated virus vectors. Hum Gene Ther 1998;9:2745 – 60.

20. Auricchio A, Hildinger M, O'connor E, Gao G, Wilson JM. Isolation of highly infectious and pure adeno-associated virus type 2 vectors with a single-step gravity-flow column. Hum Gene Ther 2001;12:71 – 6.

21. Weidner N, Folkman J, Poxxa F, et al. Tumor angiogenesis: a new significant and independent prognostic indicator in early-stage breast carcinoma. J Natl Cancer Inst 1992;84:1875 – 87.

22. Bouck N, Stellmach V, Hsu SC. How tumors become angiogenic. Adv Cancer Res 1996;69:135 – 74.

23. Hanahan D, Folkman J. Patterns and emerging mechanisms of the angiogenic switch during tumorigenesis. Cell 1996;86:353 – 64.

24. Hanahan D, Weinberg R. The hallmarks of cancer. Cell 2000;100: 57 – 70.

25. Folkman J. In: Braunwald E, et al., editors. Harrison's principles of internal medicine, 15th ed. New York (NY): McGraw-Hill; 2001. p. 517 – 30.

26. Kerbel R, Folkman J. Clinical translation of angiogenesis inhibitors. Nat Rev Cancer 2002;2:727 – 39.

27. Folkman J. Role of angiogenesis in tumor growth and metastasis. Semin Oncol 2002;29:15 – 8.

28. Wen XY, Bai Y, Stewart AK. Adenovirus-mediated human endostatin gene delivery demonstrates strain-specific antitumor activity and acute dose-dependent toxicity in mice. Hum Gene Ther 2001;12:347 – 58.

29. Jooss K, Ertl HC, Wilson JM. Cytotoxic T-lymphocyte target proteins and their major histocompatibility complex class I restriction in response to adenovirus vectors delivered to mouse liver. J Virol 1998; 72:2945 – 54.

30. Chen QR, Kumar D, Stass SA, Mixon AJ. Liposomes complexed to plasmids encoding angiostatin and endostatin inhibit breast cancer in nude mice. Cancer Res 1999;59:3308 – 12.

31. Szary J, Szala S. Intra-tumoral administration of naked plasmid DNA encoding mouse endostatin inhibits renal carcinoma growth. Int J Cancer 2001;91:835 – 9.

32. Blezinger P, Wang J, Gondo M, et al. Systemic inhibition of tumor growth and tumor metastases by intramuscular administration of the endostatin gene. Nat Biotechnol 1999;17:343 – 8.

33. Muzyczka N. Use of adeno-associated virus as a general transduction vector for mammalian cells. Curr Top Microbiol Immunol 1992;158: 97 – 129.

34. Samulski RJ, Chang LS, Shenk T. Helper-free stocks of recombinant adeno-associated viruses: normal integration does not require viral gene expression. J Virol 1989;63:3822 – 8.

35. Rabinowitz JE, Samulski J. Adeno-associated virus expression systems for gene transfer. Curr Opin Biotechnol 1998;9:470 – 5.

36. Roychowdhury DF, Tseng A, Jr., Fu KK, Weinberg V, Weidner N. New prognostic factors in nasopharyngeal carcinoma: Tumor angiogenesis and C-*erb*B2 expression. Cancer 1996;77:1419 – 26.

37. Huang GW, Masanori S, Li JE, et al. The relationship between microvessel density, the expression of vascular endothelial growth factor, and the extension of nasopharyngeal carcinoma. Laryngoscope 2000; 110:2066 – 9.

38. Rubio L, Burgos JS, Morera C, Vera-Sempere FJ. Morphometric study of tumor angiogenesis as a new prognostic factor in nasopharyngeal carcinoma patients. Pathol Oncol Res 2000;6:210 – 6.

Correction

Article on rAAC-endostatin inhibiting NPC tumor growth and metastasis

In the article on rAAC-endostatin inhibiting NPC tumor growth and metastasis in the May 2006 (1) issue, the contact information for the senior corresponding author was omitted. The appropriate information is below.

Requests for reprints: Ying Peng, Department of Neurology, The Second Affiliated Hospital, Sun Yat-Sen University, Guangzhou, 510120, China. E-mail: pengy12@yahoo.com

Reference

1. Li X-P, Li CYS, Li X, et al. Inhibition of human nasopharyngeal carcinoma growth and metastasis in mice by adenovirus-associated virus – mediated expression of human endostatin. Mol Cancer Ther 2006;5:1290 – 8.

doi:10.1158/1535-7163.MCT-06-COR2

Molecular Cancer Therapeutics

Inhibition of human nasopharyngeal carcinoma growth and metastasis in mice by adenovirus-associated virus–mediated expression of human endostatin

Xiang-Ping Li, Christine Y.S. Li, Xiaohua Li, et al.

Mol Cancer Ther 2006;5:1290-1298.